Journal of Materials Chemistry

Cite this: J. Mater. Chem., 2012, 22, 4491

www.rsc.org/materials

PAPER

Theoretical design of polythienylenevinylene derivatives for improvements of light-emitting and photovoltaic performances†

Yuqian Jiang,[a] Qian Peng,*[b] Xing Gao,[a] Zhigang Shuai,*[ab] Yingli Niu[c] and Sheng Hsien Lin[c]

Received 3rd October 2011, Accepted 15th November 2011
DOI: 10.1039/c1jm14956c

Poly(thienylene vinylene) (PTV) is a low-bandgap polymer but shows poor performance in both light-emitting and photovoltaic applications. Recently a derivative of PTV with carboxylate substitution, poly(3-carboxylated thienylenevinylene) (P3CTV), has been synthesized and was shown to be fluorescent. The photovoltaic power conversion efficiency based on P3CTV has been found to be much larger than PTV, indicating an intrinsically concomitant relationship between light-emitting and photovoltaic properties. Employing quantum chemistry calculations coupled with our correlation function formalism for excited state decay and optical spectra, we have investigated a series of side-chain substituted PTVs targeting optimal optoelectronic performance. We predict that the carbonyl substituted PTV is a strongly fluorescent polymer with low bandgap, long exciton lifetime, and large spectral overlap between emission and absorption. It is expected that carbonyl PTV is a promising light-emitting and photovoltaic polymer. Methodology wise, we find that (i) our correlation function approach to calculate the optical spectrum has much lower computational scaling with respect to the system size than the conventional method; (ii) the harmonic oscillator approximation for the nonadiabatic decay works better for a large system than for a small system.

1. Introduction

Since the discovery of conducting polymers in 1977,[1] a large variety of polymer optoelectronic devices have been demonstrated to achieve unique properties: easy and low-cost processes, controllable conductivity, light-emission, good mechanical capability, *etc.* Polymer solar cells (PSC)[2–14] have been considered as promising low-cost solar energy conversion materials, which have attracted tremendous academic and industrial interest in recent years. The most widely investigated polymers for PSC are polythiophene (PT)[15–19] and poly(1,4-phenylene vinylene) (PPV),[2,20,21] and the newly developed low band-gap donor–acceptor copolymers.[14,22,23] Poly (3-hexyl thiophene) (P3HT) is a landmark photovoltaic polymer. With the advancements in fabrication processes, the power conversion efficiencies (PCE) of P3HT:PCBM bulk heterojunction solar cells can even reach 6%.[19] However, the PCE is still limited by the relatively large bandgap (~2.0 eV) of P3HT. Hence, new low bandgap polymers have been developed over the years to achieve better spectral matching with the solar spectrum.[9–11,24–26] Copolymers based on benzo[1,2-b:3,4-b]dithiophene (BDT) with lower bandgap (1.6–1.8 eV) have been shown to reach 7.7% PCE.[27]

Poly(2,5-thienylene vinylene) (PTV) and its derivatives possess low bandgap, 1.55–1.8 eV, with large charge carrier mobility,[28,29] which become interesting potential donor materials in PSC.[10,30–38] However, the PCE of the PSC is in general very low (0.2%–0.9%), even though the absorption spectra of PTVs can cover a wide range of solar emission.[31] In order to understand why PTV-based PSCs possesses such a low PCE, Heeger and coworkers[39] have investigated an oligo(butoxyl-thienylene vinylene) (OOTV):PCBM composite by ultrafast spectroscopy. They observed a very low quantum efficiency of photoinduced electron transfer in OOTV:PCBM (less than 5%) and a very short nonradiative decay time (0.6 ps). Actually, such a fast nonradiative decay rate makes OOTV itself non-luminescent. Then, Huo *et al.*[38] have suggested a concomitant relationship between photovoltaic properties and photoluminescent properties in PTVs. They synthesized a series of PTVs and found that the PCE of PSC based on the non-luminescent

[a]*Key Laboratory of Organic OptoElectronics and Molecular Engineering, Department of Chemistry, Tsinghua University, 100084 Beijing, China. E-mail: zgshuai@tsinghua.edu.cn; Fax: +86-10-62525573; Tel: +86-10-62797689*
[b]*Key Laboratory of Organic Solids, Beijing National Laboratory for Molecular Science (BNLMS), Institute of Chemistry, Chinese Academy of Sciences, 100190 Beijing, China. E-mail: qpeng@iccas.ac.cn; Fax: +86-10-62525573; Tel: +86-10-82616830*
[c]*Department of Applied Chemistry, National Chiao Tung University, Hsinchu, 30010, Taiwan*

† Electronic supplementary information (ESI) available: full author list of ref. 88; evolution of absorption and emission spectra for COOH-PTV with temperature; ground state and excited state vibrational mode frequencies with Huang–Rhys factors for COOH-, NO_2-, and CHO-6TV; the theoretical spectra and the radiative/nonradiative decay rates of CHO-PTV resulting from the original frequencies and the new frequencies which the excited state frequency of the relative out-of-plane frequency mode is set as the same as the ground state frequency. See DOI: 10.1039/c1jm14956c

poly(3-hexyl-2,5-thienylene vinylene) (P3HTV) is as low as 0.2%, while the PCE of the luminescent poly(3-carboxylated-2,5-thienylene vinylene) (P3CTV) reaches 2%. In fact, the PTV derivatives with poor PSC performance are mostly alkyl-substituted PTVs[30–32] which are as non-luminescent as the pristine PTV.[40,41] All these experiments indicate that the luminescent property is a significant factor influencing the photovoltaic performance. It should also be noted that both PT and PPV are light-emitting. In fact, Jeeva *et al.* have synthesized a series of emissive PTV derivatives with alkylsulfanyl substituents which exhibit good electrochemical stability in field-effect transistors (FET).[42] Therefore, it is expected that improving the photoluminescence properties of PTV can enhance photovoltaic performance in PTV-based devices.

The major microscopic processes for PSC are: (i) exciton formation in the conjugated donor upon photon absorption, (ii) exciton diffusion (energy transfer) and decay, (iii) charge dissociation, (iv) charge transfer, (v) charge recombination and collection at electrodes. After exciton formation, both radiative and nonradiative decays can cause energy dissipation. Exciton diffusion is intrinsically determined by three processes: energy transfer (k_{et}), radiative decay (fluorescence, k_r), and nonradiative decay (k_{nr}). The exciton diffusion capacity can be measured by the exciton diffusion length $L_{ex} = \sqrt{ZD\tau}$, where Z is a constant relevant to spatial dimension of random walk and τ is the exciton lifetime $\tau = 1/(k_r + k_{nr})$. Under the hopping model, the diffusion coefficient D can be approximated as $D = a^2k_{et}$, where a is the intersite spacing. In the Förster energy transfer model, k_{et} is determined by the overlap between the emission and the absorption spectrum of the polymer, in addition to the electronic coupling for the exciton. Longer exciton diffusion length guarantees efficient charge dissociation. Thus, polymer emission and absorption spectra as well as exciton decay rates are essential for determining the PSC performance.

In this work, we investigate the chemical substitution effects on excited state decay rates and the optical absorption and emission spectra of PTV derivatives starting from the excited state electronic structure and the excited state-vibration coupling calculations. Krzeminski *et al.* have applied a semiempirical tight binding approach and local density approximation methods to calculate the electronic structures of the extended PTV oligomers.[43] Grozema *et al.* have calculated the electronic properties of an excited state of PTV by density functional theory methods.[44,45] However, none of these previous studies deal with the excited state decay or optical spectrum. We note that experimentally synthesized luminescent P3CTV possesses an electron-withdrawing carboxylate. We thus propose two PTV derivatives with nitryl (NO_2) and carbonyl (CHO) substituents together with experimentally available pristine PTV, alkyl PTV, carboxylated PTV and hydroxyl PTV for comparison.

In light of Kasha's rule, the excited state ordering is important for optical emission, which requires highly sophisticated electron correlation treatment for the excited state calculation. Thus we employed the multireference determinant single and double interactions coupled with Zerner's intermediate neglect of diatomic overlap (MRCI/ZINDO) method developed by our group. Peng *et al.* found that MRCI/ZINDO can give as reasonable results for excited states as the *ab initio* CASPT2 for organic molecules.[46] The substitution effect is further investigated by a simple rule proposed earlier by us based on molecular orbitals.[47] We find that the electron-withdrawing substituents –COOH, NO_2 and CHO– can dramatically change the charge distribution at the highest occupied molecular orbital (HOMO) and the lowest unoccupied molecular orbital (LUMO), which stabilize the dipole-allowed $1B_u$ state, facilitating the light emission. For those with $1B_u$ as the lowest excited state, the absorption and emission spectra as well as the radiative and nonradiative decay rates from S_1 to S_0 are calculated by the vibration correlation function formalism developed earlier by us.[48–51] In fact, Peng *et al.*[46,52,53] and Deng *et al.*[54] have applied such a formalism on several molecules and have rationalized its applicability. The theoretical spectra of COOH-PTV are in good agreement with available experimental data. The violation of mirror symmetry between emission and absorption COOH-PTV is attributed to the distortion effect between initial and final potential energy parabola. The spectra of COOH, NO_2, and CHO substituted PTVs present certain overlap between absorption and emission, ensuring energy transfer among the polymer matrix, among which the carbonyl PTV is predicted to possess a low bandgap, long excited state lifetime, and large spectral overlap of emission and absorption; namely, a very promising light-emitting and photovoltaic polymer.

2. Theoretical models and methodology

2.1. Computational model structure

Polymer structure is generally optimized by periodic boundary conditions (PBC) within density functional theory (DFT) methods.[55–58] Li *et al.*,[59–61] Collins *et al.*,[62] and Ma *et al.*[63] have developed the fragmentation method for the calculation of macromolecules to achieve low scaling computational efforts. However, all these approaches are developed for the ground state. The excited state of polymers is studied mostly based on the extrapolation of oligomers.[45,64–67] In fact, conjugated polymers present disorder or impurities, which break the conjugation. These naturally could be described as the assembly of weakly interacting conjugated segments with finite variable lengths. Taliani *et al.* have compared the electronic properties between α-sexithiophene (α-T_6) and polythiophene (PT) and concluded that α-T_6 is a model for PT.[68] Thus, in this work, we took oligo(thienylene vinylene) (OTV) as a model of PTV. Comparing the experimental spectra of different lengths of OTVs (*i.e.* nTV, $n = 2, 3, 4, 6, 8,$ and 12)[69] to that of PTV,[32,38] and considering the computation expanses for larger molecules, we chose OTV containing up to six unit cells as the model for regioregular PTV, much as in PT derivatives, see Fig. 1. Side chain substitutions include electron-withdrawing groups, NO_2 and CHO, as well as another four previously synthesized PTVs.

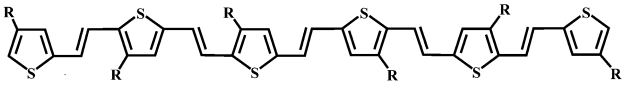

Fig. 1 OTV containing six thiophene rings.

Since the influence of alkyl groups on the conjugated backbone is very weak,[70] the side chain hexyl is replaced by methyls, and alkyls by hydrogen atoms.

2.2. Excited state structure

Kasha's rule states that the molecular fluorescence is determined by the lowest excited state symmetry. Namely, if the latter is dipole forbidden, then there is no molecular fluorescence. For excited state calculations, TDDFT is so far the most widely applied computational tool. But with the common exchange-correlation functionals, it fails to describe the excited state orderings; namely, the lowest excited state is always predicted to be an odd-parity state.[71] Highly accurate wave-function-based methods, such as complete active space self-consistent field (CASSCF) and/or its second order perturbation (CASPT2), multireference configuration interaction (MRCI) or the equation of motion coupled cluster theory (EOM-CC) should be used. However, computational costs do not allow this treatment for relatively large molecules such as ours. In recent years, several different approaches have been proposed to solve the multi-electron excitation problem within TDDFT. Dressed-TDDFT[72] and non-adiabatic TDDFT[73] focus on improvement of the behavior of the exchange-correlation kernel in the part of the strong mixing between singly and doubly excited states. Spin-flip TDDFT[74,75] and MRCI/DFT[76] methods introduce the doubly excited configurations. These have largely improved the reliability of the excited state ordering. Still, for our systems, the expensive computation problem cannot be solved by using these improved TDDFT methods either.

In fact, the semiempirical method is an alternate quantum chemistry method, especially for large conjugated hydrocarbon molecules, where parametrization has been shown to be reliable. ZINDO is the most widely applied model for excited state calculations for many conjugated polymers.[77] For obtaining correct excited state orderings and spectroscopic data, MRCI for including multiconfiguration is necessary. MRCI/ZINDO has been extensively improved by us,[78,79] and applied for rylenes recently by Peng *et al.*,[46] which gave comparable results to CASPT2.

2.3. Absorption and emission spectroscopy

Optical absorption or emission takes place between two electronic states coupled with potential energy surfaces with initial state $|\Psi_{iv_i}\rangle = |\Phi_i\Theta_{iv_i}\rangle$ and final state $|\Psi_{fv_f}\rangle = |\Phi_f\Theta_{fv_f}\rangle$, where $|\Phi_i\rangle$ and $|\Phi_f\rangle$ are the electronic states and $|\Theta_{iv_i}\rangle$ and $|\Theta_{fv_f}\rangle$ are the vibrational states. Under the harmonic approximation, the molecular vibrational state is composed of N ($3n-6$ for a nonlinear n atom molecule or $3n-5$ for a linear one) independent harmonic oscillator $|\Theta_{iv_i}\rangle = |\chi_{iv_{i1}}\chi_{iv_{i2}}\cdots\chi_{iv_{iN}}\rangle$ and $|\Theta_{fv_f}\rangle = |\chi_{fv_{f1}}\chi_{fv_{f2}}\cdots\chi_{fv_{fN}}\rangle$, where v_i and v_f are vibrational quantum numbers and $|\chi_{iv_{ik}}\rangle$and $|\chi_{fv_{fl}}\rangle$ are eigenstates of the one-dimensional harmonic oscillator Hamiltonian:

$$\hat{H}_{ik} = \frac{1}{2}\left(\hat{P}_{ik}^2 + \omega_{ik}^2\hat{Q}_{ik}^2\right) \quad (1)$$

$$\hat{H}_{fl} = \frac{1}{2}\left(\hat{P}_{fl}^2 + \omega_{fl}^2\hat{Q}_{fl}^2\right) \quad (2)$$

P and Q are the mass-weighted nuclear normal momentum operator and normal coordinate operator, respectively:

$$\hat{P}_{ik} = -i\hbar\frac{\partial}{\partial Q_{ik}} \quad (3)$$

$$\hat{P}_{fl} = -i\hbar\frac{\partial}{\partial Q_{fl}} \quad (4)$$

The normal coordinates of initial and final states can be distinguished and related by the Duschinsky rotation matrix $\boldsymbol{S}$ as:

$$Q_{ik} = \sum_{l}^{3n-6} \boldsymbol{S}_{kl}Q_{fl} + \underline{D}_k \quad (5)$$

Here D is the $(3n-6)$-dimensional normal coordinate displacement vector. $\boldsymbol{S}$ represents the mixing of normal modes in the initial and final electronic states. This is the simplest way to consider the difference in potential energy surfaces of the initial and the final states. $\boldsymbol{S}$ matrix allows different vibrational frequencies for the two potential energy parabola, the most economic way to accommodate a complicated but realistic situation. In fact, we have shown that such consideration was essential to understand the exotic aggregation induced emission phenomena in organic light emitting materials,[50,53,54] as well as the spectrum broadening and symmetry breaking.[50,80]

The absorption spectrum is defined as the absorption cross section $\sigma_{abs}(\omega, T)$ with dimensions of cm^2, which means the rate of photon energy absorption per molecule and per unit radiant energy flux. The explicit expression for $\sigma_{abs}(\omega, T)$ is given by the following formula:

$$\sigma_{abs}(\omega, T) = \frac{4\pi^2\omega}{3c}\sum_{v_i,v_f} P_{iv_i}(T)\left|\left\langle\Theta_{fv_f}\left|\boldsymbol{\mu}_{fi}\right|\Theta_{iv_i}\right\rangle\right|^2 \times\delta\left(E_{if} + E_{iv_i} - E_{fv_f} + \hbar\omega\right) \quad (6)$$

The emission spectrum is defined as the differential spontaneous photon emission rate $\sigma_{emi}(\omega, T)$ without dimension, which means the rate of spontaneous photon emission per molecule and per unit frequency between ω and $\omega + d\omega$. $\sigma_{emi}(\omega, T)$ is given by the following formula:

$$\sigma_{emi}(\omega, T) = \frac{4\omega^3}{3c^3}\sum_{v_i,v_f} P_{iv_i}(T)\left|\left\langle\Theta_{fv_f}\left|\boldsymbol{\mu}_{fi}\right|\Theta_{iv_i}\right\rangle\right|^2 \times\delta\left(E_{if} + E_{iv_i} - E_{fv_f} - \hbar\omega\right) \quad (7)$$

Here c is the velocity of light in a vacuum, ω represents the vibration frequency, and $P_{iv_i}(T)$ is the Boltzmann distribution function for the initial vibronic manifold at finite temperature. $E_{if} = E_i - E_f$ represents the adiabatic transition energy; $E_{iv_i} = \sum_k E_{iv_{ik}}$ and $E_{fv_f} = \sum_k E_{fv_{fk}}$ are the total vibrational energies in corresponding electronic states. $\boldsymbol{\mu}_{fi} = \langle\Phi_f|\boldsymbol{\mu}|\Phi_i\rangle$ is the electric transition dipole moment between two electronic states $|\Phi_i\rangle$ and $|\Phi_f\rangle$

$$\boldsymbol{\mu}_{fi} = \boldsymbol{\mu}_0 + \sum_k \boldsymbol{\mu}_\kappa Q_k + \sum_{k,l} \boldsymbol{\mu}_{kl} Q_k Q_l + \ldots \quad (8)$$

For the strongly dipole-allowed transitions of molecules, only the zeroth-order term is taken into account, the Franck–Condon (FC) approximation; while for the weakly dipole-allowed or dipole-forbidden transitions, the first-order term should be considered as well, the Herzberg–Teller (HT) effect. In this paper, the FC approximation is adopted since the light-emitting molecules are all strongly dipole-allowed transitions, even though our formalism has included the HT term.[50]

Applying the FC approximation, eqn (6) and eqn (7) can be rewritten as

$$\sigma_{\text{abs}}^{\text{FC}}(\omega, T) = \frac{4\pi^2\omega}{3\hbar c}|\boldsymbol{\mu}_0|^2 \sum_{v_i, v_f} P_{iv_i}(T) \left| \left\langle \Theta_{fv_f} \middle| \Theta_{iv_i} \right\rangle \right|^2 \delta\left(\omega_{iv_i, fv_f} - \omega\right) \quad (9)$$

$$\sigma_{\text{emi}}^{\text{FC}}(\omega, T) = \frac{4\omega^3}{3\hbar c^3}|\boldsymbol{\mu}_0|^2 \sum_{v_i, v_f} P_{iv_i}(T) \left| \left\langle \Theta_{fv_f} \middle| \Theta_{iv_i} \right\rangle \right|^2 \delta\left(\omega_{iv_i, fv_f} - \omega\right) \quad (10)$$

With Fourier transformation of the delta function, $\delta(\omega) = \frac{1}{2\pi}\int e^{i\omega t} dt$, we can obtain analytical integral formalisms for FC spectra.

$$\alpha_{\text{abs}}^{\text{FC}}(\omega) = \frac{2\pi\omega}{3\hbar c}|\boldsymbol{\mu}_0|^2 \int e^{i\omega t} e^{-iE_{fi}t/\hbar} Z_{iv}^{-1} \rho_{\text{abs},0}^{\text{FC}}(t, T) dt \quad (11)$$

$$\sigma_{\text{emi}}^{\text{FC}}(\omega) = \frac{2\omega^3}{3\pi\hbar c}|\boldsymbol{\mu}_0|^2 \int e^{-i\omega t} e^{iE_{fi}t/\hbar} Z_{iv}^{-1} \rho_{\text{emi},0}^{\text{FC}}(t, T) dt \quad (12)$$

Here,

$$\rho_{\text{abs},0}^{\text{FC}}(t, T) = Tr\left[e^{-i\tau_f \hat{H}_f} e^{-i\tau_i \hat{H}_i}\right] \quad (13)$$

$$\rho_{\text{emi},0}^{\text{FC}}(t, T) = Tr\left[e^{-i\tau_f \hat{H}_f} e^{-i\tau_i \hat{H}_i}\right] \quad (14)$$

are the thermal vibration correlation functions, in which $\tau_f = t/\hbar$, $\tau_i = -i\beta - \tau_f$, and $\beta = 1/k_B T$. $\hat{H}_{f(i)}$ is the final (initial) state Hamiltonian of multi-dimensional harmonic oscillators. Applying the path integral formula of a harmonic oscillator, the fully analytical formalisms of correlation functions can be achieved as

$$\rho^{\text{FC}}(t, T) = \sqrt{\frac{\det[\boldsymbol{a}_f \boldsymbol{a}_i]}{\det[\mathbf{K}]}} \exp\left\{ -\frac{i}{\hbar}\left[\frac{1}{2}\underline{F}^T \mathbf{K} \underline{F} - \underline{D}^T \mathbf{E} \underline{D}\right]\right\} \quad (15)$$

where $\boldsymbol{a}_i$, $\boldsymbol{a}_f$ and $\mathbf{E}$ are $N \times N$ matrices, $\mathbf{K}$ is a $2N \times 2N$ matrix, $\underline{D}$ is the $N \times 1$ column matrix, and $\underline{F}$ is the $2N \times 1$ column matrix. More details of mathematical forms are listed in ref. 50.

2.4. Radiative and nonradiative decay processes

According to the Jablonski diagram, there are three main decay pathways for S_1: (i) the radiative decay from S_1 to S_0 with a rate k_r; (ii) the nonradiative internal conversion (IC) from S_1 to S_0 with a rate k_{IC}; (iii) the intersystem crossing (ISC) process from S_1 to the first triplet excited state (T_1) with a rate K_{ISC}.

The radiative decay rate can be simply expressed as the integration over the wavelength of the light emission spectrum:

$$k_r(T) = \int_0^\infty \alpha_{\text{emi}}(\omega, T) d\omega \quad (16)$$

The IC rate can be evaluated through Fermi's golden rule presented as

$$k_{IC} = \frac{2\pi}{\hbar}\left|H'_{fi}\right|^2 \delta\left(E_{fi} + E_{fv_f} - E_{iv_i}\right) \quad (17)$$

Here the perturbation is the non-Born–Oppenheimer coupling:

$$H'_{fi} = -\hbar^2 \sum_l \left\langle \Phi_f \Theta_{fv_f} \middle| \frac{\partial \Phi_i}{\partial Q_{fl}} \frac{\partial \Theta_{iv_i}}{\partial Q_{fl}} \right\rangle \quad (18)$$

Under Condon approximation, eqn (18) is evaluated as

$$H'_{fi} = \sum_l \left\langle \Phi_f \middle| \hat{P}_{fl} \middle| \Phi_i \right\rangle \left\langle \Theta_{fv_f} \middle| \hat{P}_{fl} \middle| \Theta_{iv_i} \right\rangle \quad (19)$$

Inserting eqn (19) into eqn (17), the IC rate becomes

$$k_{IC} = \sum_{kl} k_{ic,kl} \quad (20)$$

$$k_{ic,kl} = \frac{2\pi}{\hbar} R_{kl} Z_{iv}^{-1} \sum_{v_i, v_f} e^{-\beta E_{iv_i}} P_{kl} \delta\left(E_{fi} + E_{fv_f} - E_{iv_i}\right) \quad (21)$$

Here the electronic coupling term is given as

$$R_{kl} = \left\langle \Phi_f \middle| \hat{P}_{fk} \middle| \Phi_i \right\rangle \left\langle \Phi_i \middle| \hat{P}_{fl} \middle| \Phi_f \right\rangle \quad (22)$$

and the vibrational coupling term as

$$P_{kl} = \left\langle \Theta_{fv_f} \middle| \hat{P}_{kl} \middle| \Theta_{iv_i} \right\rangle \left\langle \Theta_{iv_i} \middle| \hat{P}_{fl} \middle| \Theta_{fv_f} \right\rangle \quad (23)$$

The delta function is again Fourier transformed as

$$k_{ic,kl} = \frac{1}{\hbar^2} R_{kl} \int_{-\infty}^{\infty} dt \left[e^{i\omega_{if} t} Z_{iv}^{-1} \rho_{ic,kl}(t, T)\right] \quad (24)$$

where $\rho_{ic,kl}(\tau, T)$ is the IC correlation function,

$$\rho_{ic,kl}(t, T) = Tr\left(\hat{P}_{fk} e^{-i\tau_f \hat{H}_f} \hat{P}_{fk} e^{-i\tau_i \hat{H}_i}\right) \quad (25)$$

The analytical expression of the IC correlation function is

$$\rho_{ic,kl}(t, T) = \sqrt{\frac{\det[\boldsymbol{a}_f \boldsymbol{a}_i]}{\det[\mathbf{K}]}} \Big\{ i\hbar\left[Tr\left(\mathbf{G}_{kl}^{IC} \mathbf{K}^{-1}\right)\right] + \left(\mathbf{K}^{-1} \underline{F}^T\right) \mathbf{G}_{kl}^{IC} \left(\mathbf{K}^{-1} \underline{F}\right) - \left(\underline{H}_{kl}^{IC}\right)^T \mathbf{K}^{-1} \underline{F}\Big\} \cdot \exp\left\{ -\frac{i}{\hbar}\left[\frac{1}{2}\underline{F}^T \mathbf{K}^{-1} \underline{F} - \underline{D}^T \boldsymbol{E} \underline{D}\right]\right\} \quad (26)$$

Similar to the thermal vibration correlation function eqn (15), in IC correlation function eqn (26), $\boldsymbol{a}_i$, $\boldsymbol{a}_f$ and $\boldsymbol{E}$ are still $N \times N$ matrices, $\mathbf{K}$ is a $2N \times 2N$ matrix, $\underline{D}$ is the $N \times 1$ column matrix, while $\underline{H}$ and $\underline{F}$ are the $2N \times 1$ column matrices. More details of the IC correlation function are also given in ref. 48–51.

For the electronic coupling part of the IC rate,[48,50] we apply the first-order perturbation theory following Lin:[81]

$$\left\langle \Phi_f \middle| \frac{\partial}{\partial Q_{fl}} \middle| \Phi_i \right\rangle = \frac{\left\langle \Phi_f^0 \middle| \partial V/\partial Q_{fl} \middle| \Phi_i^0 \right\rangle}{E_i^0 - E_f^0} \quad (27)$$

$$\left\langle \Phi_f^0 \middle| \partial V/\partial Q_{fl} \middle| \Phi_i^0 \right\rangle = -\sum_\sigma \frac{Z_\sigma e^2}{\sqrt{M_\sigma}} \sum_{\tau=x,y,z} E_{j\leftarrow i,\sigma\tau} L_{\sigma\tau} \quad (28)$$

The transition electric field $E_{j\leftarrow i,\sigma\tau} = \int d\mathbf{r} \rho_{ji}(\mathbf{r}) \frac{e(r_\tau - R_{\sigma\tau})}{|\mathbf{r} - \mathbf{R}_\sigma|^3}$ can be computed directly from quantum chemistry methods.

What has to be emphasized here is that such formalism can be only applied at potential energy surfaces well away from the conical intersection points. When the conical intersection is significant, the nonadiabatic transition will become very fast with a decay rate greater than 10^{12}–10^{13} s^{-1}. Considering that the ISC rate is normally less than 10^5 s^{-1}, especially in conjugated systems, which is somewhat slower than the IC rate, only the IC rate is considered in our computation. The typical radiative decay rate is around 10^7–10^8 s^{-1}, much slower than nonadiabatic decay at a conical intersection.

2.5. Computational details

Geometry optimization and frequency calculations were carried out in the TURBOMOLE 6.0 program package.[82,83] The geometry of S_0 was optimized with DFT, while the geometry of S_1 was optimized with TDDFT. The B3LYP functional[84,85] and def2-SV(P) basis set were used in geometry optimization.[86,87] The vertical excitation energies for the three lowest-lying excited states at the optimized S_0 geometries for all OTV derivatives were calculated by MRCI/ZINDO with our own programs as well as TDDFT/B3LYP/6-31G* in the GAUSSIAN 03 program package.[88] The transition electric field for the electronic coupling term was calculated with TDDFT in GAUSSIAN 03 program package.

3. Results and discussion

3.1 Electronic structures and vertical excitation energies

The regioregular PTVs in the solid state possess a planar conformation, leading to highly conjugated backbones. Therefore, the model systems are kept planar with C_{2h} symmetry in this work. Based on the S_0 geometries optimized by B3LYP/def2-SV(P), the vertical excitation energies of the three low-lying excited states for the six PTV derivatives (Fig. 1) are calculated with TDDFT/B3LYP and MRCI/ZINDO methods, and the results are presented in Table 1. In the MRCI/ZINDO calculations, the active space contains all the occupied and unoccupied molecular orbitals (MOs) which contribute most to the excited states, and at most 12 occupied and 12 unoccupied MOs are included (Table 2). We choose six significant reference configurations, the Hartree–Fock determinant, three single-excitation configurations (HOMO → LUMO, HOMO − 1 → LUMO, and HOMO → LUMO + 1), and two double-excitation configurations (HOMO, HOMO → LUMO, LUMO and HOMO − 1, HOMO → LUMO, LUMO + 1).

Table 1 Vertical excitation energies (E_{ver}) of the three low-lying excited states at the ground state geometry for PTV derivatives and their corresponding oscillator strengths (f)

	MRCI/ZINDO		TDDFT/B3LYP	
R	E_{vert} (eV)	f	E_{vert} (eV)	f
H	A_g: 2.50	0.0000	B_u: 1.94	3.9113
	B_u: 2.76	3.1055	A_g: 2.28	0.0000
	A_g: 3.18	0.0000	A_g: 2.66	0.0000
CH_3	A_g: 2.51	0.0000	B_u: 1.93	3.9387
	B_u: 2.73	2.9759	A_g: 2.28	0.0000
	A_g: 3.12	0.0000	A_g: 2.64	0.0000
OH	A_g: 2.38	0.0000	B_u: 1.75	3.5981
	B_u: 2.41	2.2482	A_g: 2.03	0.0000
	A_g: 2.89	0.0000	A_g: 2.55	0.0000
COOH	B_u: 2.41	3.3457	B_u: 2.03	3.3678
	A_g: 2.58	0.0000	A_g: 2.32	0.0000
	A_g: 2.83	0.0000	A_g: 2.58	0.0000
NO_2	B_u: 2.45	3.0844	B_u: 2.03	2.9424
	A_g: 2.55	0.0000	A_g: 2.24	0.0000
	A_g: 2.84	0.0000	A_g: 2.51	0.0000
CHO	B_u: 2.38	3.2248	B_u: 1.96	3.1874
	A_g: 2.51	0.0000	A_g: 2.21	0.0000
	A_g: 2.77	0.0000	A_g: 2.49	0.0000

According to Kasha's rule, the MRCI/ZINDO results indicate that non-substituted PTV is nonluminescent, and the alkyl or hydroxyl substituted PTVs cannot change the excited state ordering. On the contrary, with electron-withdrawing COOH, NO_2, or CHO groups, PTVs are promising fluorescent materials. These results first justify the existing experimental evidence that COOH substituted PTV is luminescent, indicating the reliability of the MRCI/ZINDO method. Hence it is expected that NO_2 or CHO side groups can also make PTV become luminescent polymers. Nevertheless, from TDDFT/B3LYP calculations, the 1Bu state is always below the 2Ag state for all the compounds, indicating the most commonly applied B3LYP functional is qualitatively wrong for excited state ordering, because the 2Ag state mostly consists of double-excitations (HOMO, HOMO → LUMO, LUMO) added with two single excitations (HOMO − 1 → LUMO and HOMO → LUMO + 1). For the B3LYP functional, there are only single excited states included in the linear response formalism[89] and the errors in the excitation energies for these states can be as large as a few eV. However, when $1B_u$ state is indeed the lowest excited state, B3LYP is reliable for the electronic structure.

From the atomic orbital composition of the HOMO and LUMO in Fig. 2, we can find that the electronic structures of CH_3-PTV and OH-PTV are similar to non-substituted PTV, in that nearly all the electronic density distributes along the main chain backbone, while the electronic density extends partly to the side groups in COOH-PTV, NO_2-PTV, and CHO-PTV. Therefore, the fluorescence is related to the electronic structure of the orbitals.

For analysis of the substituent effects on the excited state ordering of PTV from molecular orbitals, we look at a quantity $\rho_{H/L}$ put forward by Chen *et al.*[47]

$$\rho_{\frac{H}{L}} = \frac{\sum_{\mu\in sub} |C_{H_\mu}|^2}{\sum_{\mu\in sub} |C_{L_\mu}|^2}$$

$C_{H/L}$ is the molecular orbital coefficient of the HOMO/LUMO at atomic orbital μ, and the summations only cover the orbitals

Table 2 The occupied and unoccupied molecular orbitals (MOs) included in the active space for the MRCI/ZINDO calculations in different PTVs. H represents HOMO, while L represents LUMO

	Active space	
R	Occupied	Unoccupied
H	H−14 – H−10, H−6 –H (12)	L – L + 11 (12)
CH_3	H−14 – H−10, H−6 – H (12)	L – L + 10, L + 12 (12)
OH	H−13 – H−10, H−8, H−6 – H (12)	L – L + 9, L + 12, L + 14 (12)
COOH	H−11, H−8, H−6 – H (9)	L – L + 3, L + 6, L + 11 – L + 14 (9)
NO_2	H−14, H−9 – H (11)	L – L + 3, L + 6, L + 9 – L + 14 (11)
CHO	H−17 – H−16, H−6 – H (9)	L – L + 3, L + 6, L + 11 – L + 14 (9)

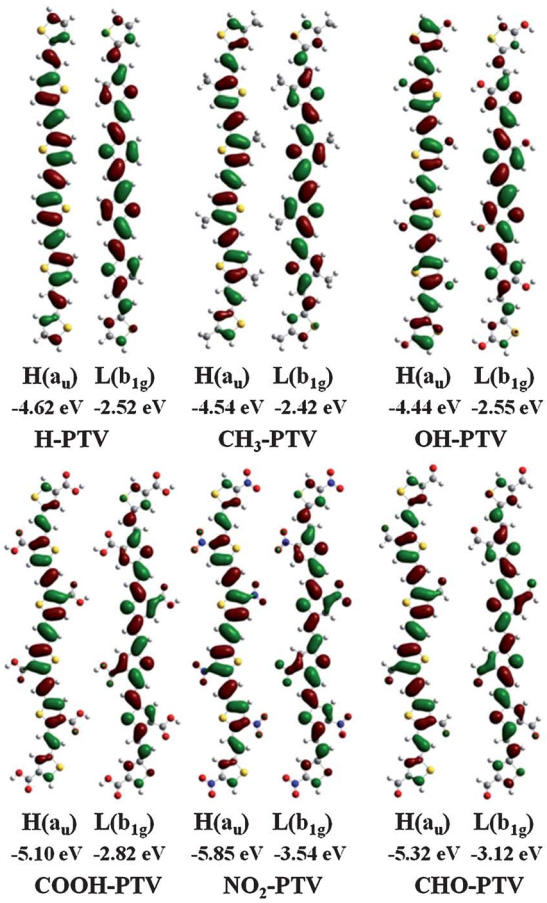

Fig. 2 The atomic orbital composition of selected molecular orbitals in PTV derivatives.

of the carbon atoms in the backbone linking the side groups. Therefore, $\rho_{H/L}$ represents the difference in charge distribution between the HOMO and LUMO induced by substituent groups. Since $1B_u$ mainly consists of the single excitation from HOMO to LUMO, the charge transfer occurring from HOMO to LUMO is significant for stabilizing the $1B_u$ state. For conjugated molecules, if the overall electron density for HOMO and LUMO are similar, then $\rho_{H/L}$ should be close to 1. This means that the substituents have little effect on the charge redistribution when an electron is excited from HOMO to LUMO. Otherwise, if $\rho_{H/L}$ deviates remarkably from 1, charge transfer from the substituent group to the main chain will obviously occur during the electron transition from HOMO to LUMO, so that the $1B_u$ can be stabilized to become the lowest-lying excited state.

The calculated ratios $\rho_{H/L}$ for six molecules are listed in Table 3. It is noted that (i) for the non-substituted PTV, CH_3-PTV and OH-PTV, their $\rho_{H/L}$ values are all close to 1, which indicates that substitutions are not able to alter the excited state ordering, namely, these materials are non-luminescent, in good agreement with available experiments; (ii) Though the OH substituent is a good electron-donating group, and it indeed induces the charge redistribution, the electron density for HOMO and LUMO are too similar, thus it could not improve the luminescent property appreciably; (iii) COOH, NO_2 and CHO substituents are strongly electron-withdrawing groups, and they all caused remarkable charge redistribution, especially in LUMO (see molecular orbitals plotted in Fig. 2). So their $\rho_{H/L}$ values deviate appreciably from 1 and fluorescence is predicted; (iv) The CHO group causes much more charge redistribution on PTV than NO_2 and COOH, though NO_2 is the strongest electron-withdrawing group among them. The results of $\rho_{H/L}$ show excellent correlation between the sophisticated electron correlation MRCI/ZINDO calculation and the simple molecular orbital calculation based on a simple rule. Therefore, it is expected that the photoluminescent properties of PTV can be improved by attaching NO_2 or CHO substituents, as is the case for the COOH substituent.

3.2. Optical spectra

Now we look at the spectral properties of the emissive polymers. TDDFT/B3LYP is employed to obtain the vibrational mode for the excited state and the ground state as well as the vibronic coupling. Keeping PTVs in C_{2h} symmetry, there is no vibrational mode with imaginary frequency for the optimized ground state structure for all three PTVs. However, there is a very small imaginary frequency existing in the optimized excited state structure for COOH-PTV and NO_2-PTV, regardless of keeping

Table 3 Calculated $\rho_{H/L}$ from the optimized geometry for different substituted OTVs, in comparison with the MRCI/ZINDO results and experimental luminescent properties: strong luminescent molecules possess a $\rho_{H/L}$ value well deviated from 1

R	H	CH3	OH	COOH	NO_2	CHO
$\rho_{H/L}$	1.29	1.20	0.91	1.51	1.40	1.85
S_1 from MRCI/ZINDO	$2A_g$	$2A_g$	$2A_g$	$1B_u$	$1B_u$	$1B_u$
Luminescence from exp.	no[a]	no[b]	no[c]	yes[b]	NA[d]	NA[d]

[a] From ref. 41. [b] From ref. 38. [c] From ref. 39. [d] Not Available.

C_{2h} symmetry or C_1 symmetry. Such a mode corresponds to the slight out-of plane motion with vanishing Huang–Rhys factor (vibronic coupling strength). Therefore, we simply replace this vibration mode in the excited state by the corresponding one in the ground state; namely, ignoring the distortion effect for this mode. Although there is no such mode for CHO-PTV, for the sake of consistency, we do the same operation for CHO-PTV so that we can compare the results. We first compute the optical spectra and decay rates of CHO-PTV with the full original modes and then replace one mode. These gave almost identical results, justifying our approach for avoiding such an imaginary frequency mode, see part 4, ESI.†

We first present the absorption and emission spectra for the experimentally available COOH-PTV at 300 K including Duschinsky effect in order to rationalize our methodology. The theoretical spectra compared with the experimental results[38] are presented in Fig. 3. Note that the broadening in the spectrum naturally originates from the coupling between the electronic excited state and all the vibration modes, without any extra broadening.

The distribution of vibration modes is closely dependent on temperature due to the Boltzmann distribution. We find the line shapes in theoretical spectra are in good agreement with the experimental results. The agreement with experiments validates the vibration correlation function theory and the electronic structure method adopted in this work.

Under the displaced harmonic oscillator model, there should exist mirror symmetry between the absorption and emission spectra, which is absent both in experiment and in theory. However, the optical spectra of COOH-PTV (Fig. 3) are not mirror symmetric in both theoretical calculation and in experimental measurement.

To understand the origin of such asymmetry, we calculate the spectra without considering the mode mixing effect, while keeping the difference in normal mode frequency between the excited state and the ground state as obtained from TDDFT (Fig. 4). We find that the structures of the spectra are nearly the same as the spectra with Duschinsky rotation effect (DRE) and the asymmetry still exists. This means the mixing of normal modes in the initial and final electronic states is not the cause of asymmetry. Therefore, the asymmetry of spectra can be ascribed

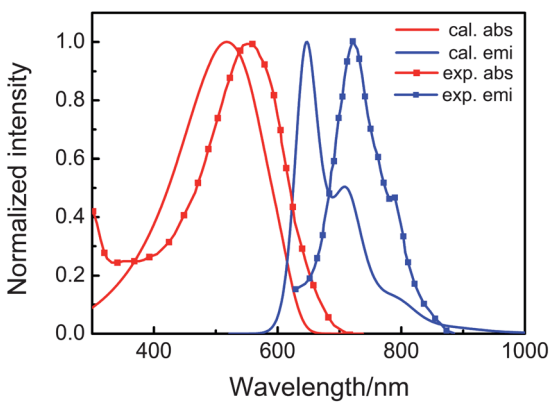

Fig. 3 Comparison of optical absorption and emission spectra between theory (T = 300 K) and experiment (in dilute $CHCl_3$ solution) for COOH-PTV.

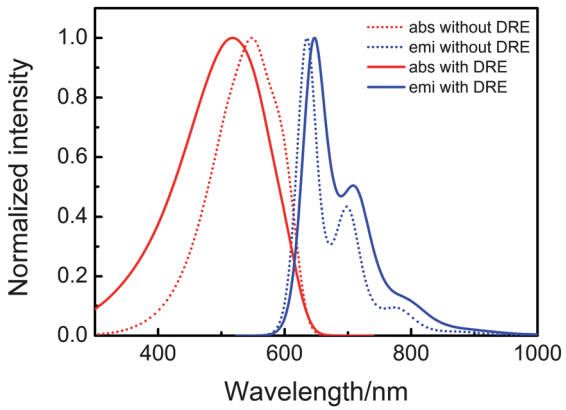

Fig. 4 The spectra of COOH-PTV with DRE compared to the spectra without DRE but with different normal mode frequency at 300 K.

to the distortion effect. The phenomena also exist in other similar systems, such as PT[66] and PPV.[67] For these flexible materials, Gierschner *et al.* ascribe the asymmetry of spectra to the enlarged torsional mobility of molecules in S_0 as compared to S_1. In the S_1 state, the C–C single bonds are shortened, so that the frequency of the torsional mode is increasing. Considering the low frequency of the torsional mode contributes most during the transition process, the difference of torsional mode frequency between S_0 and S_1 (*i.e.* distortion effect) causes the mirror symmetry of the spectra to break with increasing temperature.

Similarly, we calculate the optical spectra of NO_2-PTV and CHO-PTV, shown in Fig. 5. The absorptions peak at 518, 522, 578 nm for COOH-PTV, NO_2-PTV, and CHO-PTV respectively, while for emission, the peak positions are at 648, 663, and 678 nm correspondingly. The bandgap of CHO-PTV is indeed much lower than other compounds.

The theoretical spectra illustrate that CHO-PTV possesses a large overlap between absorption and emission spectra, helpful for faster energy transfer. Thus, theoretically we find that for CHO-PTV, the bandgap is small, the fluorescence quantum yield is large, the exciton lifetime is long, and the spectral overlap is large. All these indicate that CHO-PTV is an excellent light-emitting and photovoltaic polymer, calling for further experimental verification.

It is appropriate to discuss the advantage of our method in terms of the computational costs. Our method is based on

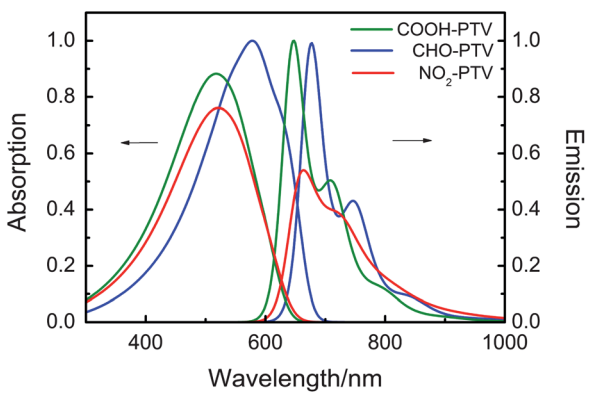

Fig. 5 Theoretical absorption and emission spectra for COOH-PTV, NO_2-PTV, and CHO-PTV.

Fourier transformation of the correlation function while the traditional approach was based on summation over vibrational states.[67,90] In sections 2.3 and 2.4, we see that all the normal modes with all the vibrational quantum numbers (from 0 to ∞) are automatically included in our formalism, in addition to considerations of the temperature effect and DRE. The exact computing time with respect to the number of normal modes for the series of COOH-nTV oligomer (n = 2–6) are presented in Fig. 6. All the computations are executed on one CPU (Intel Xeon 5420 CPU with 2.5 GHz). It is easy to find that, as the number of normal modes (N) increases, the time of computation increases approximately as N^3, related directly to the matrix manipulations. In contrast, for the traditional sum-over-states approach to emission spectrum, it is an impossible task to include all the modes with all vibrational quanta, see Appendix A for the 0 K case, and the computational costs scale as $(a + 1)^N$, where a is a cutoff of vibrational quanta. For instance, for calculations on COOH-6TV with 240 normal modes, suppose we keep only two quanta (a = 2), *i.e.* v = 0, 1, 2, and we can only keep a few "important" normal modes with appreciable Huang–Rhys factors. The computing wallclock times with respect to the number of selected modes is displayed in the inset of Fig. 6, which grows exponentially with the number of normal modes N. When N becomes greater than 24, the calculation would become too expensive even with 8 CPUs. Furthermore, such calculation does not allow consideration of the temperature effect, and in practice, the broadening of spectra has only been accomplished by hand with Gaussian or Lorentzian type functions.

3.3. Radiative and nonradiative decay rates

The formalisms for the radiative and nonradiative rate were given in section 2.3 and 2.4. We calculate the radiative rates k_r and the internal conversion rates k_{IC} for COOH, NO_2 and CHO substituted PTVs which are found to be light-emitting from MRCI/ZINDO, to study their exciton lifetime. As mentioned in section 2.4, only internal conversion is included in nonradiative decay in our work. The radiative rates k_r, internal conversion rates k_{IC}, and the exciton lifetime $\tau = 1(k_r + k_{IC})$ are listed in Table 4. It is seen that all of the three compounds possess efficient fluorescence as well as long exciton lifetime to facilitate charge dissociation.

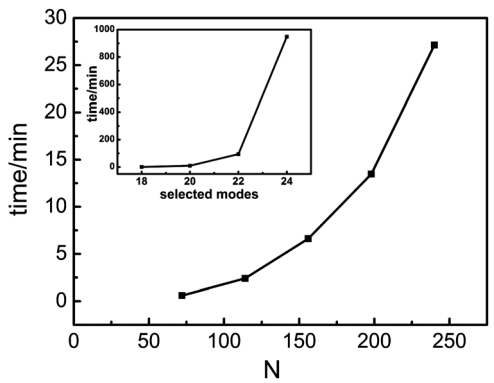

Fig. 6 The computing wall time of emission rate with respect to the number of normal modes (N) for COOH-nTV (n = 2–6) by our method. The traditional method keeping only 2 quanta is shown in the inset.

It should be noted that in our nonradiative decay rate calculation, harmonic potential energy surface approximation is adopted, which could be a severe approximation, especially for small molecules with too few degrees of freedom and a large transition band gap. For radiative decay process, the transition energy is mostly mediated by the photon energy, leaving the vibrational quanta very small. In nonradiative decay, the electronic energy of the excited state is transformed through vibrational relaxation into the final state. If the number of modes is too few and/or the transition energy is too large, the number of vibrational quanta for each mode is required to be big in order to accept the electronic energy. As a result, the anharmonicity could be important in the nonradiative decay process. However, if the number of normal modes is large enough, for instance in a conjugated polymer, many vibrational modes participate to share the electronic transition energy. Thus for any one of the modes, only a small number of vibrational quanta is required. So, for each mode, the displacement from the equilibrium is small and the harmonic model is expected to be a reasonable approximation. Hence, we expect that the harmonic model is more applicable for polymers than for molecules. To verify such a claim, we perform the following analysis on the vibrational configuration of the final state of nonradiative decay for oligomers of COOH-PTV with increasing size.

We consider the nonradiative decay process at 0 K with the promoting mode approximation. The mode with the largest electronic coupling term is regarded as the promoting mode, since it contributes the most to the IC rate. For the series of COOH-nTV oligomers (n = 2–6), we calculate the vibrational configurations when the IC rates of their promoting modes reaches the maximum values. The results are presented in Fig. 7. The analytical expression to obtain the vibrational configuration is given in Appendix B. It is clearly seen that, as the size of the system increases from 2 to 6, the vibrational quantum number responsible for nonradiative decay decreases steadily. At the same time, the adiabatic transition energy decreases due to the extension of conjugation. Namely, the harmonic oscillator model becomes more justified for conjugated polymers than for small molecules.

4. Conclusion

To conclude, we have applied a combined quantum chemistry approach to propose a theoretical design strategy to improve the optoelectronic properties of PTV. ZINDO coupled with MRCI calculations showed that COOH group substitution in PTV can lead to inversion of the excited state ordering, allowing light-emission, but CH_3 and OH groups cannot, in agreement with the existing experimental evidence. We further predict that the electron-withdrawing groups NO_2 and CHO can render PTV light-emitting, much the same as the COOH group. These results are further confirmed by molecular orbital calculations based on

Table 4 Radiative, nonradiative decay rates and exciton lifetime for the emissive substituted PTVs

R	COOH	NO_2	CHO
k_r/s^{-1}	5.25×10^8	3.94×10^8	4.50×10^8
k_{IC}/s^{-1}	1.19×10^6	2.24×10^8	2.51×10^6
τ/ns	1.90	1.62	2.21

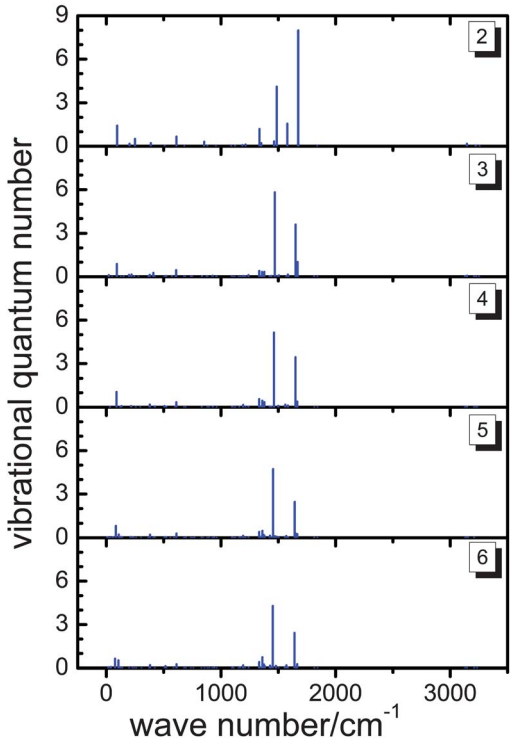

Fig. 7 The vibrational configurations of final states corresponding to the maximum IC rates under the promoting mode approximation for COOH-nTV ($n = 2$–6).

a simple rule for substitution effect on the excited state ordering, namely, their $\rho_{H/L}$ values deviate from 1 remarkably, which cause charge redistribution amongst the HOMO and LUMO and stabilize the light-emitting state $1B_u$ to be the lowest.

Starting from the lowest excited state and the ground state potential energy parabola, optical absorption and emission spectra are computed for COOH-, NO_2- and CHO-PTV through our correlation function formalism. The broken mirror symmetry for COOH-PTV found both in experiment and computation is attributed to a distortion effect; namely, the vibrational mode frequencies, in particular the low frequency parts, are different for the ground state and the excited state. The theoretical spectra of COOH-PTV are consistent with the experimental measurements. The radiative and nonradiative decay rates of the excited state for COOH-, CHO- and NO_2-PTVs are computed by the same correlation function formalism. We find that CHO-PTV possesses not only a long excited state lifetime (2.21 ns), but also a large overlap between absorption and emission spectra. These facts indicate that CHO-PTV is not only a good light-emitting polymer, but also a good photovoltaic donor material possessing long intrinsic exciton diffusion length. Although NO_2 is a stronger electron-withdrawing group than COOH or CHO, the calculations show that the spectral overlap between absorption and emission in NO_2-PTV is relatively small. Therefore, even though the excited state ordering of NO_2-PTV meets the basic requirement for molecular design, both the light emitting and photovoltaic performances are predicted to be poorer than COOH-PTV, while CHO-PTV is predicted to present better light emitting and photovoltaic performances than COOH-PTV. It is highly expected to be experimentally confirmed in the near future.

The computational costs of our correlation function formalism scale much lower with the system size than the traditional sum-over-state method. The former can further automatically take the temperature effect on the line-width broadening into account. Finally, for justifying the harmonic oscillator model for the non-radiative decay process, we analyse the number of vibrational quanta of the accepting mode. It is found that as the oligomer length increases, the number of quanta decreases. Namely the anharmonicity becomes less important for conjugated polymers than for small molecules, which rationalizes the applicability of our method for electronic polymers.

Appendix A: Conventional formalisms of radiative decay rate calculation based on sum-over-states method

At 0 K, the radiative rate can be expressed as

$$k_r(i0\rightarrow f) = \frac{4}{3\hbar c^3}|\boldsymbol{\mu}_0|^2 \sum_{v_f} \omega_{i0\rightarrow fv_f}^3 \left|\left\langle \Theta_{fv_f}\middle|\Theta_{i0}\right\rangle\right|^2 \quad \text{(A1)}$$

Under the harmonic oscillator model $\left|\Theta_{fv_f}\right\rangle = \left|\chi_{fv_{f1}}\chi_{fv_{f2}}\cdots\chi_{fv_{fN}}\right\rangle$, eqn (A1) can be expressed as

$$k_r(i0\rightarrow f) = \frac{4}{3\hbar c^3}|\boldsymbol{\mu}_0|^2 \sum_{v_f} \omega_{i0\rightarrow fv_f}^3 \prod_k \left|\left\langle \chi_{fv_k}\middle|\chi_{i0}\right\rangle\right|^2 \quad \text{(A2)}$$

Here, the Franck–Condon (FC) factor can be expressed as

$$\left|\left\langle \chi_{fv_k}\middle|\chi_{i0}\right\rangle\right|^2 = \frac{S_k^{v_k}}{v_k!}e^{-S_k} \quad \text{(A3)}$$

$$\prod_k \left|\left\langle \chi_{fv_k}\middle|\chi_{i0}\right\rangle\right|^2 = e^{-S}\prod_k{}' \frac{S_k^{v_k}}{v_k!} \quad \text{(A4)}$$

S_k, the Huang–Rhys factor of the kth mode is defined as

$$S_k = \frac{\omega_k}{2\hbar}D_k^2 \quad \text{(A5)}$$

Appendix B: The analytical expression of the vibrational configuration of the final state corresponding to the maximum IC rate under promoting mode approximation at 0 K

Neglecting temperature effect, the IC rate also can be rewritten as

$$k_{IC} = \frac{2\pi}{\hbar}\sum_v \left|\left\langle \Theta_{fv}\middle|\left\langle \Phi_f\middle|\left(\sum_k \hat{P}_k\right)\middle|\Phi_i\right\rangle\middle|\left(\sum_l \hat{P}_l\right)\Theta_{i0}\right\rangle\right|^2$$

$$\delta(E_{i0}-E_{fv}) = \sum_{k,l}\left[\frac{2\pi}{\hbar}\sum_v \left|\left\langle \Theta_{fv}\middle|\left\langle \Phi_f\middle|\hat{P}_k\middle|\Phi_i\right\rangle\middle|\hat{P}_l\Theta_{i0}\right\rangle\right|^2 \delta(E_{i0}-E_{fv})\right] \quad \text{(B1)}$$

$$k_{\mathrm{ic},kl} = \frac{2\pi}{\hbar}\sum_{v}\left|\left\langle\Theta_{\mathrm{f}v}\left|\left\langle\Phi_{\mathrm{f}}\left|\hat{P}_k\right|\Phi_{\mathrm{i}}\right\rangle\right|\hat{P}_l\Theta_{\mathrm{i}0}\right\rangle\right|^2\delta(E_{\mathrm{i}0}-E_{\mathrm{f}v}) \quad \text{(B2)}$$

With promoting mode approximation,

$$k_{\mathrm{ic},l} = \frac{2\pi}{\hbar}\sum_{v}\left|\left\langle\Theta_{\mathrm{f}v}\left|\left\langle\Phi_{\mathrm{f}}\left|\hat{P}_l\right|\Phi_{\mathrm{i}}\right\rangle\right|\hat{P}_l\Theta_{\mathrm{i}0}\right\rangle\right|^2\delta(E_{\mathrm{i}0}-E_{\mathrm{f}v})$$

$$= \frac{2\pi}{\hbar}R_{ll}\sum_{v}\left|\left\langle\Theta_{\mathrm{f}v}\left|\hat{P}_l\Theta_{\mathrm{i}0}\right\rangle\right|^2\delta(E_{\mathrm{i}0}-E_{\mathrm{f}v}) \quad \text{(B3)}$$

Here l is the promoting mode which possesses the biggest electronic coupling term.

$$\hat{P}_l = \mathrm{i}\sqrt{\frac{\hbar\omega_l}{2}}\left(\hat{a}_l^{\dagger}-\hat{a}_l\right) \quad \text{(B4)}$$

where $\hat{a}_l^{\dagger}$ and $\hat{a}_l$ are creation or annihilation operators respectively. Since the temperature is 0 K, then the contribution of annihilation $\hat{a}_l$ is 0. Then

$$k_{\mathrm{ic},l} = \pi R_{ll}\omega_l\left|\left\langle\chi_{\mathrm{f}1_l}\left|\hat{a}_l^{\dagger}\chi_{\mathrm{i}0_l}\right\rangle\right|^2\sum_{v}{}'\left[\prod_{j}{}'\left|\left\langle\chi_{\mathrm{f}v_j}\left|\chi_{\mathrm{i}0_j}\right\rangle\right|^2\right]\delta(E_{\mathrm{i}0}-E_{\mathrm{f}v})$$

$$= \pi R_{ll}\omega_l\sum_{v}{}'\left[\prod_{j}{}'\left|\left\langle\chi_{\mathrm{f}v_j}\left|\chi_{\mathrm{i}0_j}\right\rangle\right|^2\right]\delta\left[\left(E_{\mathrm{if}}-\hbar\omega_l\right)-\sum_{j}{}'v_j\hbar\omega_j\right] \quad \text{(B5)}$$

Here v is a set of vibrational configuration $\{v_1,v_2,\cdots v_{l-1},v_{l+1},\cdots v_N\}$. The δ function is the constraint condition for energy conversation. The promoting mode can only accept one phonon energy $\hbar\omega_l$, while the rest of the excited state energy transfers to accepting modes with non-zero reorganization energy.

Supposing the vibrational configuration v is a set of continuous variables, define

$$I_l(v) \equiv I_l(v_1,v_2,\cdots) \equiv \prod_{j}{}'\left|\left\langle\chi_{\mathrm{f}v_j}\left|\chi_{\mathrm{i}0_j}\right\rangle\right|^2 = \prod_{j}{}'\frac{S_j^{v_j}}{v_j!}\mathrm{e}^{-S_j} \quad \text{(B6)}$$

Under the constraint condition, $k_{\mathrm{ic},l}$ will reach its maximum when $\frac{\partial}{\partial v_j}I_l(v)=0$. Namely,

$$\frac{\partial}{\partial v_j}\ln[I_l(v)] = 0 \quad \text{(B7)}$$

To solve the equation, we introduce the Lagrange multiplier λ, and define the Lagrange function,

$$F_l(v,\lambda) = \ln[I_l(v)] + \lambda(E_{\mathrm{if}}-\hbar\omega_l-\sum_{j}{}'v_j\hbar\omega_j) \quad \text{(B8)}$$

And

$$\frac{\partial F_l(v,\lambda)}{\partial v_j} = 0 \quad \text{(B9)}$$

Using Stirling's formula:
$\ln I_l(v) = \sum_j(v_j\ln S_j - S_j - v_j\ln v_j + v_j)$, it can be expressed as

$$\frac{\partial F_l(v)}{\partial v_j} = \ln S_j - \ln v_j - \lambda\hbar\omega_j = 0 \quad \text{(B10)}$$

Thus, the vibrational quantum number of each accepting mode relevant for the maximum IC rate can be obtained by

$$v_j = S_j e^{-\lambda\hbar\omega_j} \quad \text{(B11)}$$

The total accepted energy is

$$\hbar(\omega_{fi}-\omega_l) = \sum_{j}{}'v_j\hbar\omega_j = \sum_{j}{}'\hbar\omega_j S_j e^{-\lambda\hbar\omega_j} \quad \text{(B12)}$$

So λ can be solved by

$$\omega_{fi}-\omega_l = \sum_{j}{}'\omega_j S_j e^{-\lambda\hbar\omega_j} \quad \text{(B13)}$$

Then, the vibrational configuration $\boldsymbol{v}$ relevant to the maximum IC rate under the promoting mode in eqn (B11) can be evaluated.

Acknowledgements

This work is supported by the Ministry of Science and Technology of China (Grant No. 2009CB623600) and National Science Foundation of China (Grant Nos. 20903102, 90921007). Extensive discussion on PTV with Prof. Yongfang Li has been insightful for this work.

Notes and references

1 H. Shirakawa, E. J. Louis, A. G. Macdiarmid, C. K. Chiang and A. J. Heeger, *J. Chem. Soc., Chem. Commun.*, 1977, 578–580.
2 G. Yu, J. Gao, J. C. Hummelen, F. Wudl and A. J. Heeger, *Science*, 1995, **270**, 1789–1791.
3 C. J. Brabec, S. Gowrisanker, J. J. M. Halls, D. Laird, S. J. Jia and S. P. Williams, *Adv. Mater.*, 2010, **22**, 3839–3856.
4 E. Bundgaard and F. C. Krebs, *Sol. Energy Mater. Sol. Cells*, 2007, **91**, 954–985.
5 Y. J. Cheng, S. H. Yang and C. S. Hsu, *Chem. Rev.*, 2009, **109**, 5868–5923.
6 K. M. Coakley and M. D. McGehee, *Chem. Mater.*, 2004, **16**, 4533–4542.
7 A. Facchetti, *Chem. Mater.*, 2011, **23**, 733–758.
8 S. Günes, H. Neugebauer and N. S. Sariciftci, *Chem. Rev.*, 2007, **107**, 1324–1338.
9 L. J. A. Koster, V. D. Mihailetchi and P. W. M. Blom, *Appl. Phys. Lett.*, 2006, **88**, 093511.
10 R. Kroon, M. Lenes, J. C. Hummelen, P. W. M. Blom and B. De Boer, *Polym. Rev.*, 2008, **48**, 531–582.
11 S. H. Park, A. Roy, S. Beaupre, S. Cho, N. Coates, J. S. Moon, D. Moses, M. Leclerc, K. Lee and A. J. Heeger, *Nat. Photonics*, 2009, **3**, 297–295.
12 B. C. Thompson and J. M. J. Frechet, *Angew. Chem., Int. Ed.*, 2008, **47**, 58–77.
13 X. W. Zhan and D. B. Zhu, *Polym. Chem.*, 2010, **1**, 409–419.
14 Y. Liu, Y. Q. Liu and X. W. Zhan, *Macromol. Chem. Phys.*, 2011, **212**, 428–443.
15 T. C. Chung, J. H. Kaufman, A. J. Heeger and F. Wudl, *Phys. Rev. B*, 1984, **30**, 702–710.
16 Y. Kim, S. Choulis, J. Nelson, D. Bradley, S. Cook and J. Durrant, *J. Mater. Sci.*, 2005, **40**, 1371–1376.
17 Y. Kim, S. Cook, S. M. Tuladhar, S. A. Choulis, J. Nelson, J. R. Durrant, D. D. C. Bradley, M. Giles, I. McCulloch, C.-S. Ha and M. Ree, *Nat. Mater.*, 2006, **5**, 197–203.
18 J. Y. Kim, S. H. Kim, H. H. Lee, K. Lee, W. L. Ma, X. Gong and A. J. Heeger, *Adv. Mater.*, 2006, **18**, 572–576.
19 J. Y. Kim, K. Lee, N. E. Coates, D. Moses, T. Q. Nguyen, M. Dante and A. J. Heeger, *Science*, 2007, **317**, 222–225.
20 M. M. Wienk, J. M. Kroon, W. J. H. Verhees, J. Knol, J. C. Hummelen, P. A. van Hal and R. A. J. Janssen, *Angew. Chem., Int. Ed.*, 2003, **42**, 3371–3375.
21 S. E. Shaheen, C. J. Brabec, N. S. Sariciftci, F. Padinger, T. Fromherz and J. C. Hummelen, *Appl. Phys. Lett.*, 2001, **78**, 841–843.
22 S. Ko, R. Mondal, C. Risko, J. K. Lee, S. Hong, M. D. McGehee, J.-L. Brédas and Z. Bao, *Macromolecules*, 2010, **43**, 6685–6698.

23 L. Huo, X. Guo, S. Zhang, Y. Li and J. Hou, *Macromolecules*, 2011, **44**, 4035–4037.
24 C. J. Brabec, C. Winder, N. S. Sariciftci, J. C. Hummelen, A. Dhanabalan, P. A. van Hal and R. A. J. Janssen, *Adv. Funct. Mater.*, 2002, **12**, 709–712.
25 N. Blouin, A. Michaud and M. Leclerc, *Adv. Mater.*, 2007, **19**, 2295–2300.
26 P. L. T. Boudreault, A. Najari and M. Leclerc, *Chem. Mater.*, 2011, **23**, 456–469.
27 H.-Y. Chen, J. Hou, S. Zhang, Y. Liang, G. Yang, Y. Yang, L. Yu, Y. Wu and G. Li, *Nat. Photonics*, 2009, **3**, 649–653.
28 H. Fuchigami, A. Tsumura and H. Koezuka, *Appl. Phys. Lett.*, 1993, **63**, 1372–1374.
29 C. Videlot, J. Ackermann, P. Blanchard, J. M. Raimundo, P. Frere, M. Allain, R. de Bettignies, E. Levillain and J. Roncali, *Adv. Mater.*, 2003, **15**, 306–310.
30 A. P. Smith, R. R. Smith, B. E. Taylor and M. F. Durstock, *Chem. Mater.*, 2004, **16**, 4687–4692.
31 J. Hou, Z. a. Tan, Y. He, C. Yang and Y. Li, *Macromolecules*, 2006, **39**, 4657–4662.
32 J. Y. Kim, Y. Qin, D. M. Stevens, O. Ugurlu, V. Kalihari, M. A. Hillmyer and C. D. Frisbie, *J. Phys. Chem. C*, 2009, **113**, 10790–10797.
33 M. Wan, W. Wu, G. Sang, Y. Zou, Y. Liu and Y. Li, *J. Polym. Sci., Part A: Polym. Chem.*, 2009, **47**, 4028–4036.
34 M. Horie, I. W. Shen, S. M. Tuladhar, H. Leventis, S. A. Haque, J. Nelson, B. R. Saunders and M. L. Turner, *Polymer*, 2010, **51**, 1541–1547.
35 A. Henckens, M. Knipper, I. Polec, J. Manca, L. Lutsen and D. Vanderzande, *Thin Solid Films*, 2004, **451–452**, 572–579.
36 J. Mei, N. C. Heston, S. V. Vasilyeva and J. R. Reynolds, *Macromolecules*, 2009, **42**, 1482–1487.
37 B. Lim, K.-J. Baeg, H.-G. Jeong, J. Jo, H. Kim, J.-W. Park, Y.-Y. Noh, D. Vak, J.-H. Park, J.-W. Park and D.-Y. Kim, *Adv. Mater.*, 2009, **21**, 2808–2814.
38 L. Huo, T. L. Chen, Y. Zhou, J. Hou, H.-Y. Chen, Y. Yang and Y. Li, *Macromolecules*, 2009, **42**, 4377–4380.
39 I. W. Hwang, Q. H. Xu, C. Soci, B. Chen, A. K. Y. Jen, D. Moses and A. J. Heeger, *Adv.Funct. Mater.*, 2007, **17**, 563–568.
40 A. J. Brassett, N. F. Colaneri, D. D. C. Bradley, R. A. Lawrence, R. H. Friend, H. Murata, S. Tokito, T. Tsutsui and S. Saito, *Phys. Rev. B: Condens. Matter*, 1990, **41**, 10586.
41 M. Liess, S. Jeglinski, P. A. Lane and Z. V. Vardeny, *Synth. Met.*, 1997, **84**, 891–892.
42 S. Jeeva, O. Lukoyanova, A. Karas, A. Dadvand, F. Rosei and D. F. Perepichka, *Adv. Funct. Mater.*, 2010, **20**, 1661–1669.
43 C. Krzeminski, C. Delerue, G. Allan, V. Haguet, D. Stievenard, P. Frere, E. Levillain and J. Roncali, *J. Chem. Phys.*, 1999, **111**, 6643–6649.
44 F. C. Grozema, L. P. Candeias, M. Swart, P. T. van Duijnen, J. Wildeman, G. Hadziioanou, L. D. A. Siebbeles and J. M. Warman, *J. Chem. Phys.*, 2002, **117**, 11366–11378.
45 F. C. Grozema, P. T. van Duijnen, L. D. A. Siebbeles, A. Goossens and S. W. de Leeuw, *J. Phys. Chem. B*, 2004, **108**, 16139–16146.
46 Q. Peng, Y. L. Niu, Z. H. Wang, Y. Jiang, Y. Li, Y. Liu and Z. G. Shuai, *J. Chem. Phys.*, 2011, **134**, 074510.
47 L. Chen, X. Hou, L. Zhu, S. Yin and Z. Shuai, *J. Theor. Comput. Chem.*, 2006, **5**, 391–400.
48 P. Qian, Y. Yuanping, S. Zhigang and S. Jiushu, *J. Chem. Phys.*, 2007, **126**, 114302.
49 Y. Niu, Q. Peng and Z. Shuai, *Sci. China, Ser. B: Chem.*, 2008, **51**, 1153–1158.
50 Y. Niu, Q. Peng, C. Deng, X. Gao and Z. Shuai, *J. Phys. Chem. A*, 2010, **114**, 7817–7831.
51 Q. Peng, Y. L. Niu, C. M. Deng and Z. G. Shuai, *Chem. Phys.*, 2010, **370**, 215–222.
52 Q. Peng, Y. L. Niu and Z. G. Shuai, *Chem. J. Chin. Univ.-Chin.*, 2008, **29**, 2435–2439.
53 Q. Peng, Y. P. Yi, Z. Shuai and J. Shao, *J. Am. Chem. Soc.*, 2007, **129**, 9333–9339.
54 C. M. Deng, Y. L. Niu, Q. Peng, A. J. Qin, Z. G. Shuai and B. Z. Tang, *J. Chem. Phys.*, 2011, **135**, 014304.
55 S. S. Zade and M. Bendikov, *Org. Lett.*, 2006, **8**, 5243–5246.
56 S. Pesant, P. Boulanger, M. Côté and M. Ernzerhof, *Chem. Phys. Lett.*, 2008, **450**, 329–334.
57 S. Dag and L.-W. Wang, *J. Phys. Chem. B*, 2010, **114**, 5997–6000.
58 S. S. Zade and M. Bendikov, *Chem.–Eur. J.*, 2007, **13**, 3688–3700.
59 S. Li, W. Li and T. Fang, *J. Am. Chem. Soc.*, 2005, **127**, 7215–7226.
60 W. Li, S. Li and Y. Jiang, *J. Phys. Chem. A*, 2007, **111**, 2193–2199.
61 W. J. Hua, T. Fang, W. Li, J. G. Yu and S. H. Li, *J. Phys. Chem. A*, 2008, **112**, 10864–10872.
62 V. Deev and M. A. Collins, *J. Chem. Phys.*, 2005, **122**, 154102.
63 N. Jiang, J. Ma and Y. S. Jiang, *J. Chem. Phys.*, 2006, **124**, 114112.
64 U. Salzner, *J. Chem. Theory Comput.*, 2007, **3**, 1143–1157.
65 J. E. Northrup, *Phys. Rev. B: Condens. Matter Mater. Phys.*, 2007, **76**, 245202.
66 J. Gierschner, H. G. Mack, H. J. Egelhaaf, S. Schweizer, B. Doser and D. Oelkrug, *Synth. Met.*, 2003, **138**, 311–315.
67 J. Gierschner, H.-G. Mack, L. Lüer and D. Oelkrug, *J. Chem. Phys.*, 2002, **116**, 8596.
68 C. Taliani and L. M. Blinov, *Adv. Mater.*, 1996, **8**, 353–359.
69 J. J. Apperloo, C. Martineau, P. A. van Hal, J. Roncali and R. A. J. Janssen, *J. Phys. Chem. A*, 2002, **106**, 21–31.
70 S. Hotta, S. D. D. V. Rughooputh, A. J. Heeger and F. Wudl, *Macromolecules*, 1987, **20**, 212–215.
71 A. Dreuw and M. Head-Gordon, *Chem. Rev.*, 2005, **105**, 4009–4037.
72 G. Mazur, M. Makowski, R. Wlodarczyk and Y. Aoki, *Int. J. Quantum Chem.*, 2011, **111**, 819–825.
73 O. V. Gritsenko and E. J. Baerends, *Phys. Chem. Chem. Phys.*, 2009, **11**, 4640–4646.
74 Z. Rinkevicius, O. Vahtras and H. Agren, *J. Chem. Phys.*, 2010, **133**, 114104.
75 Y. H. Shao, M. Head-Gordon and A. I. Krylov, *J. Chem. Phys.*, 2003, **118**, 4807–4818.
76 S. Grimme and M. Waletzke, *J. Chem. Phys.*, 1999, **111**, 5645–5655.
77 G. R. Hutchison, M. A. Ratner and T. J. Marks, *J. Phys. Chem. A*, 2002, **106**, 10596–10605.
78 Y. P. Yi, L. Y. Zhu and Z. G. Shuai, *J. Chem. Phys.*, 2006, **125**, 164505.
79 Y. P. Yi, Q. X. Li, L. Y. Zhu and Z. G. Shuai, *J. Phys. Chem. A*, 2007, **111**, 9291–9298.
80 C. M. Deng, Y. L. Niu, Q. Peng and Z. G. Shuai, *Acta Phys.-Chim. Sin.*, 2010, **26**, 1051–1058.
81 S. H. Lin, *Rate of Interconversion of Electronic and Vibrational Energy*. AIP: 1966; Vol. 44, p 3759–3767.
82 P. Deglmann and F. Furche, *J. Chem. Phys.*, 2002, **117**, 9535–9538.
83 P. Deglmann, F. Furche and R. Ahlrichs, *Chem. Phys. Lett.*, 2002, **362**, 511–518.
84 C. Lee, W. Yang and R. G. Parr, *Phys. Rev. B*, 1988, **37**, 785.
85 A. D. Becke, *J. Chem. Phys.*, 1993, **98**, 5648–5652.
86 A. Schafer, H. Horn and R. Ahlrichs, *J. Chem. Phys.*, 1992, **97**, 2571–2577.
87 F. Weigend and R. Ahlrichs, *Phys. Chem. Chem. Phys.*, 2005, **7**, 3297–3305.
88 M. J. Frisch, *et al.*, *Gaussian 03, Revision C.02*; Gaussian Inc.: Wallingford CT, 2004.
89 R. J. Cave, F. Zhang, N. T. Maitra and K. Burke, *Chem. Phys. Lett.*, 2004, **389**, 39–42.
90 G. Heimel, *J. Chem. Phys.*, 2005, **122**, 054501.